

# Design-Specification Tiling for ICL-based CAD Code Generation

Yali Du, San-Zhuo Xi, Hui Sun, Ming Li

National Key Laboratory for Novel Software Technology, School of Artificial Intelligence,  
Nanjing University, China

{duyl, xisz, sunh, lim}@lamda.nju.edu.cn

## Abstract

Large language models (LLMs) have demonstrated remarkable capabilities in code generation, yet they underperform on domain-specific tasks such as Computer-Aided Design (CAD) code generation due to scarce training data. In-Context Learning (ICL) offers a training-free alternative through task-specific exemplars. However, existing selection strategies prioritize similarity or point-wise diversity, often producing redundant selections that fail to satisfy the compositional requirements of complex CAD design specifications. In this work, we propose *knowledge sufficiency* as a principled objective for exemplar selection that aims to maximally satisfy all requirements within design specifications. To realize this objective, we introduce *Design-Specification Tiling (DST)*, which quantifies knowledge sufficiency through a surrogate tiling ratio by extracting multi-granular design components and measuring the proportion of query components covered by selected exemplars. We demonstrate that maximizing this objective constitutes submodular maximization and provide a polynomial-time greedy algorithm with a  $(1-1/e)$ -approximation guarantee. Extensive experiments demonstrate that DST substantially improves CAD code generation quality, consistently outperforming existing exemplar selection strategies in ICL.

## 1 Introduction

Computer-Aided Design (CAD) serves as a cornerstone of the engineering design process in traditional manufacturing, bridging conceptual designs with precise 3D objects through underlying code that enables model customization and automation. However, designing complex models in professional CAD software presents substantial challenges, even for highly experienced practitioners. Consequently, leveraging AI to automatically generate CAD code represents a promising avenue for advancing manufacturing capabilities [Khan *et al.*, 2024; Alam and Ahmed, 2024].

Recent advances in large language models (LLMs) have demonstrated remarkable capabilities in code generation [Liu *et al.*, 2025a; Yang *et al.*, 2024; Lyu *et al.*, 2025; Wang *et*

*al.*, 2025a], motivating their application to CAD code generation [Guan *et al.*, 2025; Niu *et al.*, 2025]. However, unlike general-purpose programming languages, CAD code is domain-specific, tightly coupled to specialized software, involves precise dimensions and physical constraints, and is typically hidden behind a GUI. Most engineers interact with CAD exclusively through visual interfaces, yet the software fundamentally relies on underlying code to generate and modify geometry. Because CAD code remains largely inaccessible to practitioners and is rarely documented or shared publicly, training corpora for this domain are scarce. Therefore, LLMs exhibit inferior performance on CAD code generation tasks, such as Qwen3-30B-A3B, which yields only 15.67% syntactically valid CAD code for complex tasks in a zero-shot setting (as shown in Tab. 1).

Most existing approaches address this challenge by continually fine-tuning open-source LLMs on manually annotated CAD datasets [Doris *et al.*, 2025; He *et al.*, 2025; Guan *et al.*, 2025]. However, these approaches face fundamental limitations: fine-tuning demands substantial computational resources, while manual annotation is costly and high-quality proprietary designs remain confidential, ultimately limiting dataset scale and quality. Recently, In-Context Learning (ICL) has emerged as a training-free alternative that enhances LLM performance by incorporating task-specific exemplars directly into the input context [Li *et al.*, 2024; Koike *et al.*, 2024; Du *et al.*, 2025]. This approach enables leveraging state-of-the-art (SOTA) models (including open and closed-source LLMs) without requiring access to training infrastructure or large-scale datasets.

The effectiveness of ICL depends critically on selecting appropriate exemplars. However, exemplar selection for CAD code generation remains largely unexplored. Selecting appropriate exemplars for natural language design-specification poses significant challenges. CAD design specifications typically comprise multiple geometric elements, spatial relationships, and topological constraints, requiring exemplars that provide sufficient information across these multiple dimensions. Existing ICL methods focus primarily on similarity [Lee *et al.*, 2025; Singh *et al.*, 2025; Ma *et al.*, 2025] or point-wise diversity [Kapuriya *et al.*, 2025; Xiao *et al.*, 2025], often resulting in redundant selections or multi-objective balance, that fail to collectively cover the compositional requirements of complex design specifications.

In this work, we return to first principles of ICL: *exemplar selection should provide sufficient task-relevant knowledge to enable LLMs to solve the current task*. Motivated by this principle, we propose **knowledge sufficiency** as a novel objective for exemplar selection that aims to maximally satisfy all requirements within design specifications of the current query. However, two practical key challenges arise: 1) How to quantify the sufficiency of a group selected exemplars? 2) How to maximize this sufficiency score with exemplar selection despite it is NP-hard?

To address these challenges, we propose an approach termed **Design-Specification Tiling (DST)** that quantifies and maximizes knowledge sufficiency through a surrogate objective. For the first challenge, DST extracts multi-granular design components from design specifications using n-grams. DST then tiles the current query’s design components using components from selected exemplars. The proportion of covered components, named **tiling ratio**, serves as a surrogate measure of knowledge sufficiency. For the second challenge, we demonstrate that maximizing this surrogate objective constitutes submodular maximization. While finding the optimal solution is NP-hard, a greedy algorithm provides an efficient solution: starting with an empty set, it iteratively selects exemplars that maximize marginal gain until reaching capacity. This greedy approach has been proven to achieve a  $(1 - 1/e)$ -approximation guarantee in polynomial time, meaning its performance is at least  $(1 - 1/e)$  of optimal.

Our main contributions are summarized as follows:

- **Knowledge Sufficiency: A Principled Objective for ICL.** We propose knowledge sufficiency as a novel objective that maximally satisfies design specification requirements within the query, thereby maximizing task-relevant knowledge provided to LLMs.
- **Design-Specification Tiling Ratio: A Tractable Surrogate Objective.** We quantify knowledge sufficiency via multi-granular design-specification tiling ratio, which extracts n-gram design components and measures the proportion of query components covered by exemplars.
- **Greedy Submodular Maximization: An efficient Solution with Approximation Guarantees.** We demonstrate this NP-hard optimization problem is submodular and provide a polynomial-time greedy algorithm with a  $(1 - 1/e)$ -approximation guarantee.

## 2 Preliminaries

In this section, we formulate ICL-based CAD code generation and articulate the key challenges that motivate our approach.

### 2.1 ICL-based CAD Code Generation

Given a natural language design specification  $X$  describing the CAD model,  $X$  typically encompasses multiple aspects of the target model, including geometric elements (*e.g.*, cylinders, spheres), spatial relationships (*e.g.*, adjacent, centered), and topological constraints (*e.g.*, union, intersection). The goal of CAD code generation is to use an LLM to transform the specification into executable CAD code:  $X_{\text{query}} \xrightarrow{\text{LLM}} \hat{Y}$ ,

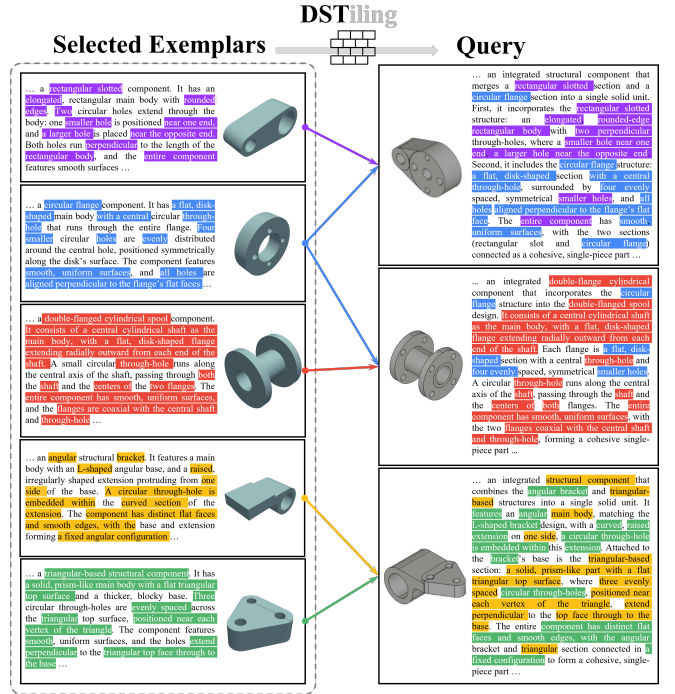


Figure 1: Compositional complexity in CAD design-specifications. The query (right) contains multiple design components (colored highlights), each requiring specific knowledge. Exemplars (left) each cover different component subsets. Effective selection should ensure collective coverage across all components.

where  $\hat{Y}$  realizes the specified design and enables CAD software to render the corresponding digital model.

In ICL, a database  $\mathcal{D} = \{(X_i, Y_i)\}_{i=1}^n$  contains  $n$  pairs of design specifications and their CAD code. The database indices are denoted by  $\mathbb{N}_n = \{1, 2, \dots, n\}$ , and  $S \subseteq \mathbb{N}_n$  represents a subset of indices. Thus, ICL-based CAD code generation with  $k$  exemplars as context can be expressed as:

$$\text{prompt}[\underbrace{X_{S[1]}, Y_{S[1]}, \dots, X_{S[k]}, Y_{S[k]}}_{S: \text{context of } k \text{ paired exemplars}}, X_{\text{query}}] \xrightarrow{\text{LLM}} \hat{Y}, \quad (1)$$

where  $S[i]$  denotes the index of the  $i$ -th selected exemplar.

### 2.2 Motivated Objective: Knowledge Sufficiency

The effectiveness of ICL depends on selecting appropriate exemplars that provide sufficient task-relevant knowledge to the LLM. However, existing strategies face key limitations when applied to CAD code generation. CAD design specifications comprise various heterogeneous components (*e.g.*, geometric elements, spatial relationships, and topological constraints), each requiring different types of knowledge.

Fig. 1 illustrates this compositional complexity. The query (right) combines multiple distinct design elements: rectangular slotted structures, circular flanges, double-flanged cylinders, angular brackets, and triangular bases. Mainstream ICL methods select the top- $k$  most similar exemplars, often producing redundant selections that cover overlapping components while missing others [Ma *et al.*, 2025;

Li *et al.*, 2025b]. Recent approaches incorporate diversity constraints but optimize for point-wise diversity without considering collective coverage of the query’s compositional requirements [Kapuriya *et al.*, 2025; Xiao *et al.*, 2025].

We return to the first principle of ICL: *providing sufficient task-relevant knowledge to enable the LLM to solve the current task*. We formalize this through knowledge sufficiency: selecting exemplars that collectively cover all components of the query. Formally, we seek an exemplar set  $S^*$  of size  $k$  that maximizes:

$$S^* = \operatorname{argmax}_{S \subseteq \mathbb{N}_n, |S|=k} f_{\text{suff}}(S; X_{\text{query}}), \quad (2)$$

where  $f_{\text{suff}}(S; X_{\text{query}})$  quantifies the knowledge sufficiency provided by  $S$  for query  $X_{\text{query}}$ .

This objective presents two practical challenges: (1) How to measure knowledge sufficiency? (2) How to efficiently search the exponential space of  $\binom{n}{k}$  possible sets? These challenges motivate DST (Sec. 3), which quantifies sufficiency through multi-granular component tiling and leverages submodular optimization to find an efficient solution.

### 3 Method: Design-Specification Tiling (DST)

To operationalize the ideal knowledge sufficiency objective, we propose Design-Specification Tiling (DST), which addresses both the quantification and optimization challenges through a surrogate objective. The core insight of DST is to measure knowledge sufficiency through the *tiling ratio*: decomposing design specifications into multi-granular components and quantifying the proportion of query components that are tiled by selected exemplars. This tiling ratio serves as a computable surrogate for knowledge sufficiency, a higher ratio indicates that exemplars collectively provide more comprehensive knowledge about the query’s requirements.

DST operates in three stages: **(1)** Extract multi-granular design-specification components from natural language using n-grams (Sec. 3.1); **(2)** Formulate the tiling ratio as a surrogate objective that measures how well exemplar components tile the query components (Sec. 3.2); **(3)** Optimize this objective efficiently via submodular maximization (Sec. 3.3).

#### 3.1 Multi-Granular Specification Components

To compute the tiling ratio, we introduce a structured representation that decomposes design specifications into *multi-granular components*. This representation enables quantifying the semantic overlap between queries and exemplars at multiple levels of granularity, from atomic design elements to complex compositional patterns.

Given a natural language design specification  $X$ , we extract components using n-grams of varying sizes. An n-gram of size  $n$  captures a consecutive sequence of  $n$  words, representing a design element at a specific semantic granularity. Unigrams such as “cylinder” capture atomic geometric primitives, while trigrams such as “cylinder with holes” capture compositional relationships between elements. This multi-granular representation is critical for CAD specifications, which inherently describe designs at multiple levels, from individual geometric shapes to their spatial arrangements and topological operations. Formally, we apply a sliding window of size  $n$  to extract all consecutive n-grams from

specification  $X$ . The set of n-grams of size  $n$  is defined as:

$$\mathcal{C}^{(n)}(X) = \{X[i : i + n] \mid i = 1, 2, \dots, L - n + 1\}, \quad (3)$$

where  $X[i : i + n]$  denotes the n-gram starting at position  $i$ .

Moreover, to capture design knowledge across semantic levels, we extract n-grams for exponentially spaced sizes  $N = \{2, 4, 8, 16, 32\}$ .

The complete component set is:

$$\mathcal{C}(X) = \bigcup_{n \in N} \mathcal{C}^{(n)}(X). \quad (4)$$

For  $i$ -th exemplar with specification  $X_i$ , we denote its component set as  $\mathcal{C}_i = \mathcal{C}(X_i)$ . For query  $X_{\text{query}}$ , we denote its component set as  $\mathcal{C}_{\text{query}} = \mathcal{C}(X_{\text{query}})$ . This exponential spacing balances expressiveness with computational efficiency, capturing design elements from local word pairs to longer compositional phrases while avoiding exhaustive enumeration of all intermediate sizes.

#### 3.2 Tiling Ratio

Having extracted multi-granular components, we now formulate the tiling ratio as a tractable surrogate for knowledge sufficiency. The key idea is to measure what proportion of the query’s components are tiled by components from selected exemplars. For an exemplar set  $S \subseteq \mathbb{N}_n$ , the union of components from all selected exemplars is:

$$\mathcal{C}(S) = \bigcup_{i \in S} \mathcal{C}_i. \quad (5)$$

The components that tile the query are those shared between the exemplar set and the query:  $\mathcal{C}(S) \cap \mathcal{C}_{\text{query}}$ . The tiling ratio quantifies the proportion of query components that are tiled:

$$f_{\text{suff}}(S; X_{\text{query}}) := \frac{w(\mathcal{C}(S) \cap \mathcal{C}_{\text{query}})}{w(\mathcal{C}_{\text{query}})}. \quad (6)$$

Here  $w(\mathcal{C}(X)) = \sum_{n \in N} n \cdot |\mathcal{C}^{(n)}(X)|$  is the weighted tiling of components in  $X$ , where longer specification components receive proportionally higher weight, thus encoding the disparate impact of multi-granularity specifications. This ratio ranges from 0 (no query components are tiled) to 1.0 (all query components are tiled). A higher tiling ratio indicates that the selected exemplars collectively provide knowledge about more aspects of the query.

Our goal is to select  $k$  exemplars that maximize the tiling ratio. Since  $|\mathcal{C}_{\text{query}}|$  is constant for a given query, maximizing the tiling ratio is equivalent to maximizing the number of tiled query components:

$$S^* = \operatorname{arg} \max_{S \subseteq \mathbb{N}_n, |S|=k} w(\mathcal{C}(S) \cap \mathcal{C}_{\text{query}}), \quad (7)$$

where  $k$  is the exemplar set capacity, a hyperparameter that controls the number of selected exemplars.

This formulation follows our knowledge sufficiency principle: we seek exemplars whose components, when combined, tile the maximum portion of the query’s compositional structure. However, this optimization involves searching an exponential space of  $\binom{n}{k}$  possible exemplar combinations.

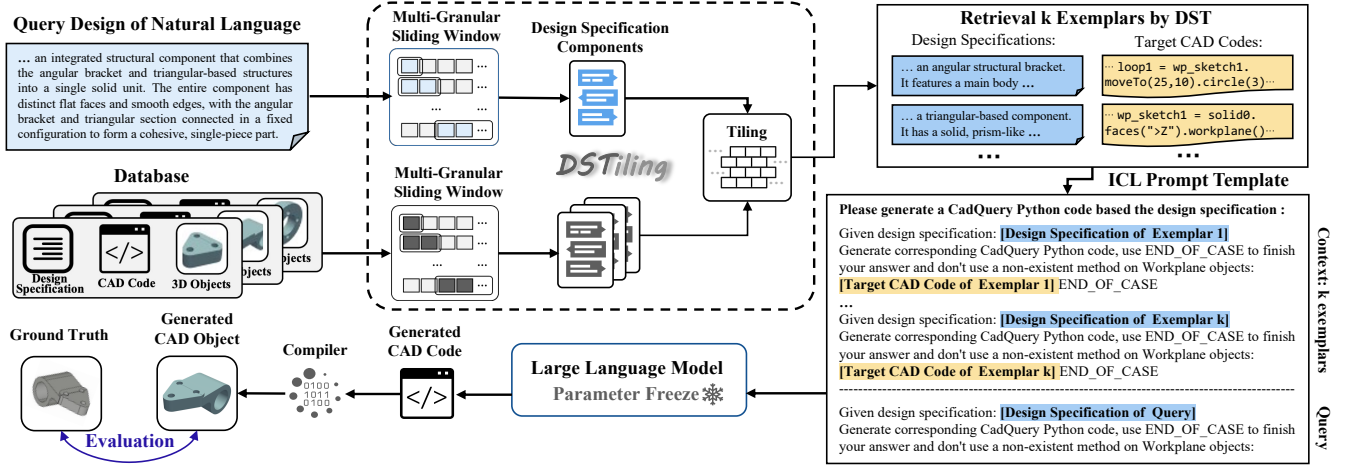


Figure 2: Overview of the Design-Specification Tiling (DST) framework. Design specification components are extracted from the query and database using multi-granular sliding windows (left). The DST retrieval algorithm selects  $k$  exemplars that maximize coverage of query components through greedy optimization (center). Selected exemplars are formatted into an ICL prompt template to guide the large language model in generating CAD code, which is then compiled and evaluated (right).

### 3.3 Efficient Submodular Maximization

The optimization problem in Eq. (7) requires selecting  $k$  exemplars from an exponential search space of  $\binom{n}{k}$  possibilities, which is computationally intractable for exhaustive search. We address this challenge by leveraging the submodular structure of the tiling objective, which enables efficient approximation with provable guarantees.

We first establish the key structural property of our objective function through the concept of submodularity.

**Definition 1** (Submodularity [Nemhauser and Wolsey, 1978]). A set function  $f : 2^\Omega \rightarrow \mathbb{R}_{\geq 0}$  is submodular if for all  $A \subseteq B \subseteq \Omega$  and  $x \in \Omega \setminus B$ :

$$f(A \cup \{x\}) - f(A) \geq f(B \cup \{x\}) - f(B), \quad (8)$$

and  $f$  is monotone if  $f(A) \leq f(B)$  for all  $A \subseteq B \subseteq \Omega$ .

Intuitively, submodularity captures the diminishing returns property: adding an exemplar to a smaller set provides at least as much benefit as adding it to a larger set, since the larger set likely already contains overlapping components.

**Proposition 1.** The tiling objective  $f(S) = |\mathcal{C}(S) \cap \mathcal{C}_{\text{query}}|$  satisfies the following properties:

- *Non-negativity:*  $f(S) \geq 0$  for all  $S \subseteq \mathbb{N}_n$ ;
- *Monotonicity:*  $f(A) \leq f(B)$  for all  $A \subseteq B$ ;
- *Submodularity:* For all  $A \subseteq B$  and  $x \notin B$ ,  $f(A \cup \{x\}) - f(A) \geq f(B \cup \{x\}) - f(B)$ .

The proof is provided in Appendix A.

These properties enable the application of efficient greedy algorithms with strong theoretical guarantees. For non-negative, monotone submodular functions, a greedy selection strategy achieves near-optimal performance [Sun *et al.*, 2025; Du *et al.*, 2025], as formalized in the following theorem.

**Theorem 1** ( $(1 - 1/e)$ -Approximation [Nemhauser and Wolsey, 1978]). For a non-negative, monotone submodular

function  $f$ , the greedy algorithm that iteratively selects elements maximizing marginal gain produces a solution  $\hat{S}$  of size  $k$  satisfying:

$$\begin{aligned} f(\hat{S}) &\geq \left(1 - \left(1 - \frac{1}{k}\right)^k\right) f(S^*) \\ &\geq \lim_{k \rightarrow +\infty} \left(1 - \left(1 - \frac{1}{k}\right)^k\right) f(S^*) = \left(1 - \frac{1}{e}\right) f(S^*), \end{aligned} \quad (9)$$

where  $S^* = \arg \max_{S \subseteq \Omega, |S| \leq k} f(S)$  is the optimal solution.

Based on this theorem, our algorithm starts with an empty set  $S = \emptyset$  and iteratively selects the exemplar with maximum marginal gain:

$$i^* = \operatorname{argmax}_{i \in \mathbb{N}_n \setminus S} [w(\mathcal{C}(S \cup \{i\}) \cap \mathcal{C}_{\text{query}}) - w(\mathcal{C}(S) \cap \mathcal{C}_{\text{query}})] \quad (10)$$

adding  $i^*$  to  $S$  in each iteration. This continues until  $|S| = k$  or no exemplar provides positive marginal gain.

The greedy algorithm runs in polynomial time, with complexity depending on the efficiency of the component set operations. Importantly, the  $(1 - 1/e) \approx 0.63$  approximation guarantee ensures that our solution achieves at least 63% of the optimal tiling ratio. For monotone submodular maximization under a cardinality constraint  $k$ , a tighter bound of  $1 - (1 - 1/k)^k$  can be derived. For typical values such as  $k = 3$ , this yields  $1 - (2/3)^3 \approx 70.4\%$ .

### 3.4 Overall Framework

Fig. 2 shows the complete DST framework, which operates in two main stages: exemplar retrieval and code generation.

In the retrieval stage, given a natural language query  $X_{\text{query}}$ , we first extract its design specification components  $\mathcal{C}_{\text{query}}$  using multi-granular sliding windows (Eq. (4)). We then apply our DST algorithm to select  $k$  exemplars  $S^* \subseteq \mathbb{N}_n$  that maximize the tiling ratio  $f_{\text{TR}}(S^*, X_{\text{query}})$  over the database. This

Table 1: Performance of LLMs with various ICL exemplar strategies (5-shot).

|              | Strategy          | Easy           |                |                 |                  | Middle         |                |                 |                  | Hard           |                |                 |                  |
|--------------|-------------------|----------------|----------------|-----------------|------------------|----------------|----------------|-----------------|------------------|----------------|----------------|-----------------|------------------|
|              |                   | VSR $\uparrow$ | IoU $\uparrow$ | CD $\downarrow$ | ECD $\downarrow$ | VSR $\uparrow$ | IoU $\uparrow$ | CD $\downarrow$ | ECD $\downarrow$ | VSR $\uparrow$ | IoU $\uparrow$ | CD $\downarrow$ | ECD $\downarrow$ |
| /3-30B-A3B   | Zero-Shot         | 0.5267         | 0.2609         | 0.6133          | 0.4877           | 0.2933         | 0.1274         | 0.6788          | 0.5354           | 0.1567         | 0.0738         | 0.6587          | 0.5593           |
|              | Random            | 0.7400         | 0.5056         | 0.3978          | 0.3481           | 0.6467         | 0.3942         | 0.4294          | 0.3550           | 0.4133         | 0.2228         | 0.4889          | 0.4393           |
|              | LDSIM             | 0.8233         | 0.5260         | 0.3607          | 0.3330           | 0.6733         | 0.4200         | 0.3964          | 0.3391           | 0.5033         | 0.2660         | 0.4610          | 0.4068           |
|              | Diversity         | 0.7867         | 0.5136         | 0.3925          | 0.3479           | 0.6467         | 0.3741         | 0.4435          | 0.3742           | 0.6067         | 0.3216         | 0.4067          | 0.3690           |
|              | BM25              | 0.6733         | 0.4982         | 0.4144          | 0.3670           | 0.6567         | 0.4228         | 0.4050          | 0.3416           | <b>0.6767</b>  | 0.3621         | 0.3867          | 0.3535           |
|              | <b>DST (Ours)</b> | <b>0.8333</b>  | <b>0.5387</b>  | <b>0.3316</b>   | <b>0.3112</b>    | <b>0.6967</b>  | <b>0.4280</b>  | <b>0.3944</b>   | <b>0.3366</b>    | 0.6667         | <b>0.3827</b>  | <b>0.3639</b>   | <b>0.3344</b>    |
|              | Improv.(%)        | 1.21           | 2.41           | 8.07            | 6.55             | 3.48           | 1.23           | 0.50            | 0.74             | -1.48          | 5.69           | 5.9             | 5.4              |
| epSeek-V3    | Zero-Shot         | 0.4900         | 0.2524         | 0.6709          | 0.5184           | 0.5000         | 0.2309         | 0.5472          | 0.4338           | 0.3833         | 0.1769         | 0.5633          | 0.4742           |
|              | Random            | 0.9467         | 0.7694         | 0.1041          | 0.1769           | 0.9100         | 0.6829         | 0.1502          | 0.1874           | 0.7900         | 0.4947         | 0.2516          | 0.2524           |
|              | LDSIM             | 0.9667         | 0.8003         | 0.0907          | 0.1682           | 0.9267         | 0.6985         | 0.1440          | 0.1782           | <b>0.9067</b>  | 0.5570         | 0.1913          | 0.2086           |
|              | Diversity         | <b>0.9767</b>  | 0.7959         | 0.0818          | 0.1612           | 0.9067         | 0.6715         | 0.1566          | 0.1840           | 0.8867         | 0.5263         | 0.2139          | 0.2235           |
|              | BM25              | 0.9167         | 0.7687         | 0.1193          | 0.1932           | 0.9133         | 0.7051         | 0.1439          | 0.1849           | 0.8700         | 0.5586         | 0.2009          | 0.2123           |
|              | <b>DST (Ours)</b> | <b>0.9767</b>  | <b>0.8227</b>  | <b>0.0778</b>   | <b>0.1580</b>    | <b>0.9367</b>  | <b>0.7083</b>  | <b>0.1229</b>   | <b>0.1646</b>    | 0.8900         | <b>0.5905</b>  | <b>0.1807</b>   | <b>0.1988</b>    |
|              | Improv.(%)        | 0.00           | 2.80           | 4.89            | 1.99             | 1.08           | 0.45           | 14.59           | 7.63             | -1.84          | 5.71           | 5.54            | 4.70             |
| ide4.5-Haiku | Zero-Shot         | 0.6867         | 0.3681         | 0.4372          | 0.3828           | 0.7100         | 0.3930         | 0.3770          | 0.3161           | 0.4667         | 0.1973         | 0.5096          | 0.4401           |
|              | Random            | 0.9900         | 0.6669         | 0.1084          | 0.1815           | 0.9867         | 0.604          | 0.1432          | 0.1754           | 0.9467         | 0.5138         | 0.2215          | 0.2266           |
|              | LDSIM             | <b>0.9933</b>  | <b>0.7090</b>  | 0.1027          | 0.1772           | <b>0.9900</b>  | 0.6159         | 0.1369          | 0.1707           | 0.9333         | 0.5097         | 0.2197          | 0.2247           |
|              | Diversity         | 0.9867         | 0.6475         | 0.1187          | 0.1862           | 0.9767         | 0.5876         | 0.1451          | 0.1770           | <b>0.9533</b>  | 0.5033         | 0.2103          | 0.2160           |
|              | BM25              | 0.9900         | 0.7085         | 0.0992          | 0.1758           | 0.9833         | 0.6310         | 0.1348          | 0.1645           | 0.9400         | 0.5110         | 0.2045          | 0.2171           |
|              | <b>DST (Ours)</b> | <b>0.9933</b>  | 0.7039         | <b>0.0975</b>   | <b>0.1757</b>    | <b>0.9900</b>  | <b>0.6590</b>  | <b>0.1156</b>   | <b>0.1554</b>    | 0.9433         | <b>0.5253</b>  | <b>0.2037</b>   | <b>0.2108</b>    |
|              | Improv.(%)        | 0.00           | -0.72          | 1.71            | 0.06             | 0.00           | 4.44           | 14.24           | 5.53             | -1.05          | 2.24           | 0.39            | 2.41             |

$\uparrow$ : Higher value indicates better performance (VSR/IoU);  $\downarrow$ : Lower value indicates better performance (CD/ECD).

<sup>2</sup> *Improv.(%)* represents the performance improvement percentage of DST over the the best result excluding DST itself.

greedy selection process leverages pre-computed component sets  $\{C_i\}_{i=1}^n$  for all database exemplars to efficiently identify the most complementary examples.

In the generation stage, the selected exemplars and their corresponding CAD code are organized into an ICL prompt, with each exemplar formatted as a specification-code pair. The query’s specification is then appended to this prompt. A LLM with frozen parameters processes this prompt to generate the target CAD code, which is subsequently compiled and executed to render the final digital model. The pseudocode of the algorithm is detailed in Appendix ??.

## 4 Experiment

We conduct extensive experiments to demonstrate the effectiveness of the proposed method.

### 4.1 Experimental protocol

**Dataset.** We adopt the widely used Text2CAD dataset [Khan *et al.*, 2024], including 178K samples. After filtering entries with missing inputs and removing duplicates, it retains 151K valid samples. To evaluate LLM on CAD code generation tasks of varying complexity, we sort samples by intrinsic metrics (specification length, geometric complexity, and lines of executable CAD code) and split them into three complexity-based subsets: Easy, Middle, and Hard. From each subset, we randomly select 300 samples as the test set, with the remainder serving as the in-context learning database.

**Baselines.** We compare against SOTA LLMs, including the open-source Qwen3 [Yang *et al.*, 2025], DeepSeek-V3 [Liu *et al.*, 2024], and the closed-source Claude 4.5-Haiku [Anthropic, 2025]. To evaluate the effectiveness of

DST, we compare against various exemplar selection strategies following the previous works [Chen *et al.*, 2023; Xiao *et al.*, 2025; Du *et al.*, 2025] for ICL: 1) Zero-shot, 2) Random Sampling, 3) Similarity-based Sampling, including Retrieval by Levenshtein Distance Similarity (LDSIM), Retrieval by Best Matching 25 (BM25), and 4) Diversity-based Sampling.

**Evaluation Metrics.** We directly evaluate the 3D objects rendered from LLM-generated CAD code. Specifically, we employ four quantitative metrics: (1) Valid Syntax Rate (VSR), which measures the compilation success rate of generated CAD code; (2) Intersection over Union (IoU), which quantifies volumetric overlap by computing the ratio of intersection to union between generated and ground-truth objects; (3) Chamfer Distance (CD), which measures point cloud similarity through bidirectional nearest-neighbor distances; (4) Edge Chamfer Distance (ECD), which applies Chamfer Distance specifically to edge point clouds for enhanced sensitivity to geometric features such as corners and sharp edges. We utilize the Python-based CadQuery library<sup>1</sup> as the CAD compiler for rendering 3D objects from generated code. Additional details on data processing, baselines, and metrics are provided in Appendices B, D, and E.2.

### 4.2 Quantitative Analysis

#### ✿ RQ 1. How does DST compare to baseline strategies across different LLMs?

As shown in Tab. 1, DST consistently outperforms all baselines across three LLMs (Qwen3-30B-A3B, DeepSeek-V3, and Claude 4.5-Haiku). DST achieves the highest VSR/IoU

<sup>1</sup><https://cadquery.readthedocs.io/>

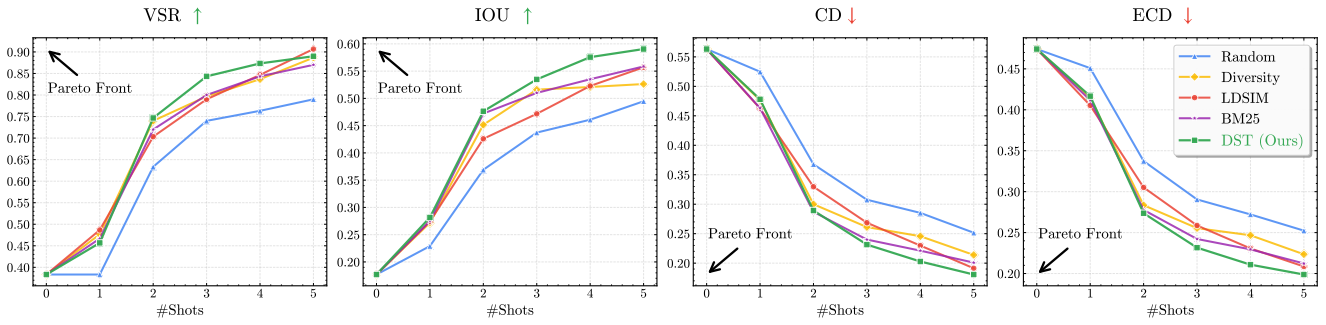


Figure 3: Performance trends of ICL strategies with increasing shot numbers based on DeepSeek-V3 on Hard tasks (Pareto front analysis)

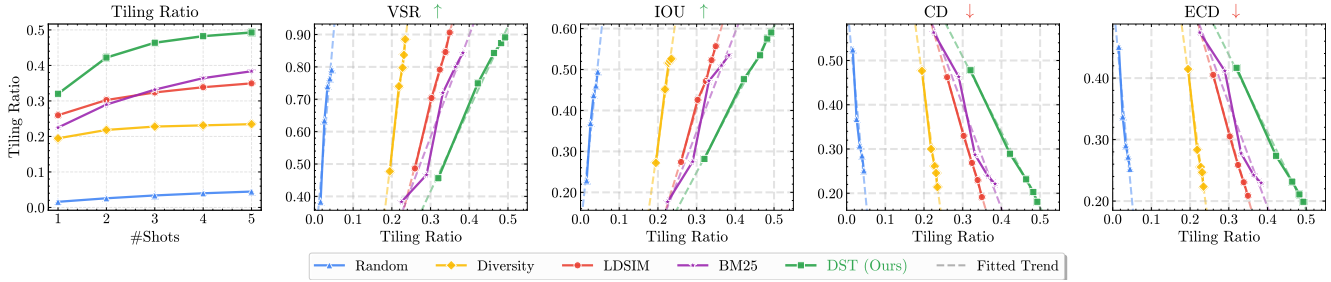


Figure 4: Correlation between Tiling Ratio, Shot Count, and Performance on DeepSeek-V3 on Hard tasks across different ICL strategies

and the lowest CD/ECD in most tasks, with significant improvements across metrics. This superiority shows that DST can provide sufficient task-relevant knowledge through optimized exemplar selection. Besides, all ICL strategies outperform the zero-shot baseline, confirming that exemplar demonstrations effectively supplement CAD domain knowledge.

#### ⚙️ RQ 2. How does task difficulty affect DST results?

DST provides greater benefits for Middle complex tasks. In Tab. 1, while all ICL strategies improve performance across difficulty levels, DST’s advantages are most pronounced for Middle tasks. Compared to the best baseline on DeepSeek-V3, DST reduces CD by 14.59% on Middle tasks, larger than 4.89% and 5.54% improvement on Easy and Hard tasks. This indicates that demonstrations help LLMs manage complex design logic and avoid syntactic/structural errors in moderately challenging tasks, yet LLMs already perform well on simple tasks and still struggle to grasp and apply knowledge for overly complex tasks, even with demonstrations.

#### ⚙️ RQ 3. How does model performance scale with the number of in-context exemplars?

As shown in Fig. 3, DST approaches the Pareto front more efficiently than baselines across all metrics. With 3 shots, DST achieves 0.54 IoU, while Diversity requires 5 shots to reach comparable performance (0.53 IoU). Diminishing marginal returns emerge for all strategies when shot count exceeds 2, as task-relevant knowledge approaches sufficiency. However, DST exhibits a steeper upward trajectory: each added exemplar introduces novel information not covered by previous selections, while similarity-based baselines select redundant content that fails to expand information.

#### ⚙️ RQ 4. How does tiling ratio relate to performance?

As shown in Fig. 4, DST’s tiling ratio consistently sur-

passes that of baselines, increasing steadily from  $\sim 0.3$  to  $\sim 0.5$  across 1–5 shots, while baselines show limited growth (left panel). This shows that DST effectively optimizes the surrogate metric of knowledge sufficiency. Critically, a strong linear correlation exists between tiling ratio and performance across all strategies (four right panels). This validates tiling ratio as an effective surrogate metric for knowledge sufficiency, confirming that optimizing tiling ratio directly improves CAD code generation performance.

### 4.3 Qualitative Analysis (Case Study)

#### ⚙️ RQ 5. How do exemplars selected by DST differ from baseline strategies?

Fig. 5 illustrates exemplar selection by DST and the best baseline LDSIM for CAD design specification. For the first specification with two key features (“cylinder with hole” and “protruding rod”), LDSIM captures only “cylinder with hole” while missing “protruding rod.” For the second specification with three key features (“circular hole,” “oval shape,” and “tray”), LDSIM captures “hole” and “oval” but misses “tray.” In contrast, DST selects exemplars that tiles all features in both cases. This demonstrates that the similarity top- $k$  approach (LDSIM) retrieves homogeneous exemplars with incomplete coverage, while DST selects complementary exemplars that provide sufficient compositional knowledge.

#### ⚙️ RQ 6. How does generation quality change with increasing exemplar shots?

Fig. 6 compares generated CAD objects from DST and the best baseline LDSIM across four tasks with increasing exemplar shots. DST consistently generates models closely matching ground truth in shape, topology, and features. In contrast, LDSIM outputs exhibit structural flaws: fragmentation,

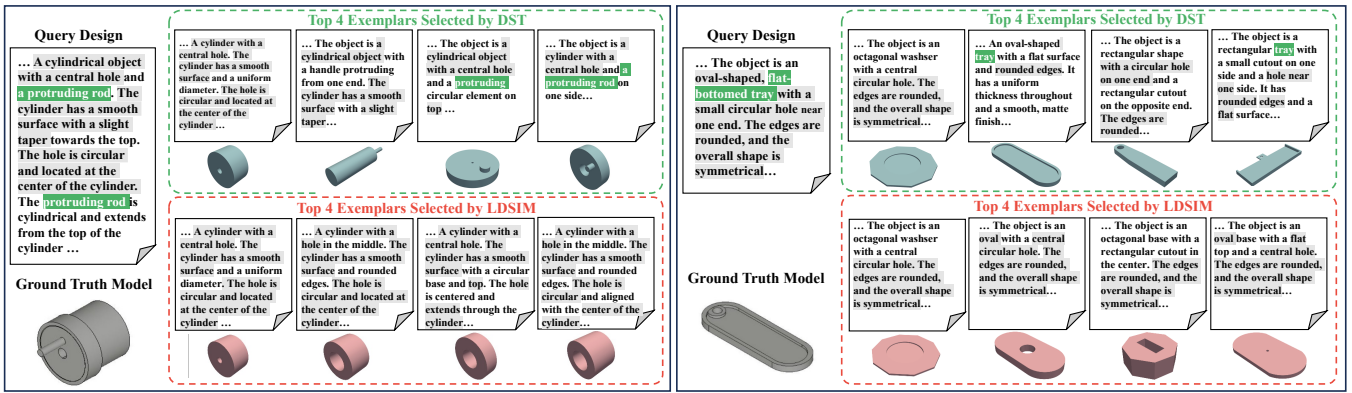


Figure 5: Exemplar Selection Quality Comparison Between DST and LDSIM for CAD Code Generation

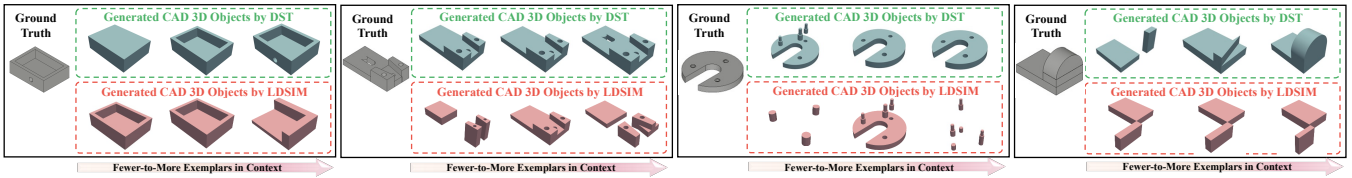


Figure 6: Generated CAD Object Quality Comparison of DST vs. LDSIM with Fewer-to-More In-Context Exemplars

missing holes, and extraneous geometry. As exemplar shot increases, DST-generated objects outputs progressively converge toward the ground truth, while LDSIM shows instability: in three left three cases, outputs degrade with additional exemplars due to redundant selections. This occurs because LDSIM’s similarity-based selection retrieves redundant exemplars that fail to provide novel guidance, while DST consistently selects complementary exemplars that incrementally expand knowledge coverage and improve generation quality.

## 5 Related Works

**CAD Code Generation.** With the advancement of generated AI, CAD code generation has emerged as a hot research field. Its core goal is to generate precise, editable 3D models directly from design specification, outperforming traditional 3D reconstruction method by enabling parametric control and design flexibility [Koch *et al.*, 2019]. Existing approaches employ diverse modalities and technical designs: 1) **Img2CAD**: Xu *et al.*, [2024], Alam *et al.*, [2024] used vision-language models map image inputs to CAD commands; Wang *et al.*, [2025b] introduced flexible code formats to enhance modeling expressiveness. 2) **Text2CAD**: Compared to Img2CAD, Text2CAD has emerged as a prominent recent trend, owing to the fact that formal visual input is not only more challenging to acquire but also less generalizable than natural language design intent. Khan *et al.*, [2024] used encoder-decoder architectures to translate textual descriptions into command sequences. Guan *et al.*, [2025] leveraged CadQuery improve the precision of LLM-based CAD code generation by integrating chain-of-thought reasoning and geometric reward mechanisms.

**LLMs for Code Generation.** Traditional code generation tasks primarily tackled by seq-to-seq models opti-

mized via supervised fine-tuning [Svyatkovskiy *et al.*, 2020; Le *et al.*, 2022; Li *et al.*, 2022; Zheng *et al.*, 2023] suffered from limited generalization and high computational overhead for parameter updates as the model parameters increased. The rise of LLMs has reshaped code generation paradigms, expanding real-world applications from function-level code generation [Fakhoury *et al.*, 2024] to full-stack project scaffolding [Zhang *et al.*, 2024]. The research efforts of code generation focusing on training-free strategies to boost performance, such as chain-of-thought [Li *et al.*, 2025a; Yang *et al.*, 2024], code ranking [Zhang *et al.*, 2023; Lyu *et al.*, 2025], in-context learning [Li *et al.*, 2025b], combining compiler testing [Fakhoury *et al.*, 2024], etc. These strategies have pushed the performance of advanced code LLMs (e.g., CodeLlama [Roziere *et al.*, 2023], DeepSeek-Coder [Guo *et al.*, 2024]) well beyond that of traditional methods.

## 6 Conclusions and Future Directions

This work addresses the underperformance of LLMs in domain-specific CAD code generation by introducing knowledge sufficiency as a principled objective for ICL exemplar selection. To optimize the objective, we propose DST, a submodular framework that quantifies component coverage via a tiling ratio, and leverages greedy optimization with a  $(1 - 1/e)$  approximation guarantee. Extensive experiments demonstrate that DST consistently outperforms existing strategies across multiple LLMs and task difficulties, validating knowledge sufficiency as an effective objective. This work opens promising future directions: extending to other compositional generation tasks, enriching the tiling framework with learned semantic similarity, adapting to hierarchical program structures, and exploring how LLMs integrate compositional knowledge for next-generation frameworks.

## References

- [Alam and Ahmed, 2024] Md Ferdous Alam and Faez Ahmed. Gencad: Image-conditioned computer-aided design generation with transformer-based contrastive representation and diffusion priors. *arXiv preprint arXiv:2409.16294*, 2024.
- [Alrashedy *et al.*, 2025] Kamel Alrashedy, Pradyumna Tambwekar, Zulfiqar Haider Zaidi, Megan Langwasser, Wei Xu, and Matthew C. Gombolay. Generating CAD code with vision-language models for 3d designs. In *The Thirteenth International Conference on Learning Representations*, 2025.
- [Anthropic, 2025] Anthropic. Claude haiku 4.5 system card. <https://assets.anthropic.com/m/99128ddd009bdcdb/Claude-Haiku-4-5-System-Card.pdf>, 2025.
- [Chen *et al.*, 2023] Shiqi Chen, Yiran Zhao, Jinghan Zhang, I-Chun Chern, Siyang Gao, Pengfei Liu, and Junxian He. FELM: benchmarking factuality evaluation of large language models. In *Advances in Neural Information Processing Systems* 36, 2023.
- [Doris *et al.*, 2025] Anna C Doris, Md Ferdous Alam, Amin Heyrani Nobari, and Faez Ahmed. Cad-coder: An open-source vision-language model for computer-aided design code generation. In *International Design Engineering Technical Conferences and Computers and Information in Engineering Conference*, 2025.
- [Du *et al.*, 2025] Yali Du, Hui Sun, and Ming Li. Post-incorporating code structural knowledge into pretrained models via icl for code translation. *IEEE Transactions on Software Engineering*, 51(11):3038–3055, 2025.
- [Fakhoury *et al.*, 2024] Sarah Fakhoury, Aaditya Naik, Georgios Sakkas, Saikat Chakraborty, and Shuvendu K Lahiri. Llm-based test-driven interactive code generation: User study and empirical evaluation. *IEEE Transactions on Software Engineering*, 2024.
- [Feng *et al.*, 2020] Zhangyin Feng, Daya Guo, Duyu Tang, Nan Duan, Xiaocheng Feng, Ming Gong, Linjun Shou, Bing Qin, Ting Liu, Daxin Jiang, and Ming Zhou. CodeBERT: A pre-trained model for programming and natural languages. In *Findings of the Association for Computational Linguistics*, pages 1536–1547, 2020.
- [Guan *et al.*, 2025] Yandong Guan, Xilin Wang, Ximing Xing, Jing Zhang, Dong Xu, and Qian Yu. Cad-coder: Text-to-cad generation with chain-of-thought and geometric reward. *arXiv preprint arXiv:2505.19713*, 2025.
- [Guo *et al.*, 2024] Daya Guo, Qihao Zhu, Dejian Yang, Zhenda Xie, Kai Dong, Wentao Zhang, Guanting Chen, Xiao Bi, Yu Wu, YK Li, et al. Deepseek-coder: When the large language model meets programming—the rise of code intelligence. *arXiv preprint arXiv:2401.14196*, 2024.
- [He *et al.*, 2025] Changqi He, Shuhan Zhang, Liguozhang, and Jiajun Miao. Cad-coder: Text-guided cad files code generation. *arXiv preprint arXiv:2505.08686*, 2025.
- [Kapuriya *et al.*, 2025] Janak Kapuriya, Manit Kaushik, Debasis Ganguly, and Sumit Bhatia. Exploring the role of diversity in example selection for in-context learning. In *Proceedings of the 48th International ACM SIGIR Conference on Research and Development in Information Retrieval*, pages 2962–2966, 2025.
- [Khan *et al.*, 2024] Mohammad S Khan, Sankalp Sinha, Talha U Sheikh, Didier Stricker, Sk A Ali, and Muhammad Z Afzal. Text2cad: Generating sequential cad designs from beginner-to-expert level text prompts. *Advances in Neural Information Processing Systems* 37, pages 7552–7579, 2024.
- [Koch *et al.*, 2019] Sebastian Koch, Albert Matveev, Zhongshi Jiang, Francis Williams, Alexey Artemov, Evgeny Burnaev, Marc Alexa, Denis Zorin, and Daniele Panozzo. Abc: A big cad model dataset for geometric deep learning. In *Proceedings of the IEEE/CVF conference on computer vision and pattern recognition*, pages 9601–9611, 2019.
- [Koike *et al.*, 2024] Ryuto Koike, Masahiro Kaneko, and Naoaki Okazaki. OUTFOX: Llm-generated essay detection through in-context learning with adversarially generated examples. In *Proceedings of the AAAI Conference on Artificial Intelligence*, pages 21258–21266, 2024.
- [Le *et al.*, 2022] Hung Le, Yue Wang, Akhilesh Deepak Gotmare, Silvio Savarese, and Steven Chu Hong Hoi. Coderl: Mastering code generation through pretrained models and deep reinforcement learning. *Advances in Neural Information Processing Systems* 35, pages 21314–21328, 2022.
- [Lee *et al.*, 2025] Seung Hyun Lee, Jijun Jiang, Yiran Xu, Zhuofang Li, Junjie Ke, Yinxiao Li, Junfeng He, Steven Hickson, Katie Datsenko, Sangpil Kim, et al. Cropper: Vision-language model for image cropping through in-context learning. In *Proceedings of the Computer Vision and Pattern Recognition Conference*, pages 30010–30019, 2025.
- [Li *et al.*, 2022] Yujia Li, David Choi, Junyoung Chung, Nate Kushman, Julian Schrittwieser, Rémi Leblond, Tom Eccles, James Keeling, Felix Gimeno, Agustin Dal Lago, et al. Competition-level code generation with alphacode. *Science*, 378(6624):1092–1097, 2022.
- [Li *et al.*, 2024] Guozheng Li, Peng Wang, Jiajun Liu, Yikai Guo, Ke Ji, Ziyu Shang, and Zijie Xu. Meta in-context learning makes large language models better zero and few-shot relation extractors. In *Proceedings of the Thirty-Third International Joint Conference on Artificial Intelligence*, pages 6350–6358, 2024.
- [Li *et al.*, 2025a] Jia Li, Ge Li, Yongmin Li, and Zhi Jin. Structured chain-of-thought prompting for code generation. *ACM Transactions on Software Engineering and Methodology*, 34(2):1–23, 2025.
- [Li *et al.*, 2025b] Jia Li, Chongyang Tao, Jia Li, Ge Li, Zhi Jin, Huangzhao Zhang, Zheng Fang, and Fang Liu. Large language model-aware in-context learning for code generation. *ACM Transactions on Software Engineering and Methodology*, 34(7):1–33, 2025.
- [Lian *et al.*, 2013] Zhouhui Lian, Afzal Godil, Xianfang Sun, and Jianguo Xiao. Cm-bof: Visual similarity-

- based 3d shape retrieval using clock matching and bag-of-features. *Machine Vision and Applications*, 24, 11 2013.
- [Liu *et al.*, 2024] Aixin Liu, Bei Feng, Bing Xue, Bingxuan Wang, Bochao Wu, Chengda Lu, Chenggang Zhao, Chengqi Deng, Chenyu Zhang, Chong Ruan, *et al.* Deepseek-v3 technical report. *arXiv preprint arXiv:2412.19437*, 2024.
- [Liu *et al.*, 2025a] Ren-Biao Liu, Anqi Li, Chaoding Yang, Hui Sun, and Ming Li. Revisiting chain-of-thought in code generation: Do language models need to learn reasoning before coding? In *Proceedings of the 42nd International Conference on Machine Learning*, volume 267, pages 38809–38826, 2025.
- [Liu *et al.*, 2025b] Ye Liu, Yuqing Niu, Chengyan Ma, Ruidong Han, Wei Ma, Yi Li, Debin Gao, and David Lo. Towards secure program partitioning for smart contracts with llm’s in-context learning. *arXiv preprint arXiv:2502.14215*, 2025.
- [Lyu *et al.*, 2025] Zhicun Lyu, Xinye Li, Zheng Xie, and Ming Li. Top pass: improve code generation by pass@k-maximized code ranking. *Frontiers of Computer Science*, 19(8):198341, 2025.
- [Ma *et al.*, 2025] Xuetao Ma, Wenbin Jiang, and Hua Huang. Problem-solving logic guided curriculum in-context learning for llms complex reasoning. In *Findings of the Association for Computational Linguistics, ACL*, pages 8394–8412, 2025.
- [Nemhauser and Wolsey, 1978] George L Nemhauser and Laurence A Wolsey. Best algorithms for approximating the maximum of a submodular set function. *Mathematics of operations research*, 3(3):177–188, 1978.
- [Niu *et al.*, 2025] Ke Niu, Haiyang Yu, Zhuofan Chen, Mengyang Zhao, Teng Fu, Bin Li, and Xiangyang Xue. From intent to execution: Multimodal chain-of-thought reinforcement learning for precise cad code generation. *arXiv preprint arXiv:2508.10118*, 2025.
- [Roziere *et al.*, 2023] Baptiste Roziere, Jonas Gehring, Fabian Gloeckle, Sten Sootla, Itai Gat, Xiaoqing Ellen Tan, Yossi Adi, Jingyu Liu, Romain Sauvestre, Tal Remez, *et al.* Code llama: Open foundation models for code. *arXiv preprint arXiv:2308.12950*, 2023.
- [Shen *et al.*, 2025] Chen Shen, Jin Wang, Sajjadur Rahman, and Eser Kandogan. Magesql: Enhancing in-context learning for text-to-sql applications with large language models. *arXiv preprint arXiv:2504.02055*, 2025.
- [Singh *et al.*, 2025] Aaditya K. Singh, Ted Moskovitz, Sara Dragutinovic, Felix Hill, Stephanie C. Y. Chan, and Andrew M. Saxe. Strategy cooperation explains the emergence and transience of in-context learning. In *Forty-second International Conference on Machine Learning*, 2025.
- [Sun *et al.*, 2025] Hui Sun, Shiyin Lu, Huanyu Wang, Qing-Guo Chen, Zhao Xu, Weihua Luo, Kaifu Zhang, and Ming Li. MDP3: A training-free approach for list-wise frame selection in video-LLMs. *arXiv preprint arXiv:2501.02885*, 2025.
- [Svyatkovskiy *et al.*, 2020] Alexey Svyatkovskiy, Shao Kun Deng, Shengyu Fu, and Neel Sundaresan. Intellicode compose: Code generation using transformer. In *Proceedings of the 28th ACM joint meeting on European software engineering conference and symposium on the foundations of software engineering*, pages 1433–1443, 2020.
- [Wang *et al.*, 2025a] Chong Wang, Jian Zhang, Yebo Feng, Tianlin Li, Weisong Sun, Yang Liu, and Xin Peng. Teaching code llms to use autocompletion tools in repository-level code generation. *ACM Transactions on Software Engineering and Methodology*, 34(7):1–27, 2025.
- [Wang *et al.*, 2025b] Xilin Wang, Jia Zheng, Yuanhao Hu, Hao Zhu, Qian Yu, and Zihan Zhou. From 2d CAD drawings to 3d parametric models: A vision-language approach. In *Proceedings of the AAAI Conference on Artificial Intelligence*, pages 7961–7969, 2025.
- [Wu *et al.*, 2021] Rundi Wu, Chang Xiao, and Changxi Zheng. Deepcad: A deep generative network for computer-aided design models. In *Proceedings of the IEEE/CVF International Conference on Computer Vision*, pages 6772–6782, 2021.
- [Xiao *et al.*, 2025] Wenyang Xiao, Haoyu Zhao, and Lingxiao Huang. The role of diversity in in-context learning for large language models. *arXiv preprint arXiv:2505.19426*, 2025.
- [Xu *et al.*, 2024] Jingwei Xu, Chenyu Wang, Zibo Zhao, Wen Liu, Yi Ma, and Shenghua Gao. Cad-mllm: Unifying multimodality-conditioned cad generation with mllm. *arXiv preprint arXiv:2411.04954*, 2024.
- [Yang *et al.*, 2024] Guang Yang, Yu Zhou, Xiang Chen, Xiangyu Zhang, Terry Yue Zhuo, and Taolue Chen. Chain-of-thought in neural code generation: From and for lightweight language models. *IEEE Transactions on Software Engineering*, 2024.
- [Yang *et al.*, 2025] An Yang, Anfeng Li, Baosong Yang, Beichen Zhang, Binyuan Hui, Bo Zheng, Bowen Yu, Chang Gao, Chengen Huang, Chenxu Lv, *et al.* Qwen3 technical report. *arXiv preprint arXiv:2505.09388*, 2025.
- [Zhang *et al.*, 2023] Tianyi Zhang, Tao Yu, Tatsunori Hashimoto, Mike Lewis, Wen-tau Yih, Daniel Fried, and Sida Wang. Coder reviewer reranking for code generation. In *International Conference on Machine Learning*, pages 41832–41846, 2023.
- [Zhang *et al.*, 2024] Kechi Zhang, Jia Li, Ge Li, Xianjie Shi, and Zhi Jin. Codeagent: Enhancing code generation with tool-integrated agent systems for real-world repository-level coding challenges. In *Proceedings of the 62nd Annual Meeting of the Association for Computational Linguistics*, pages 13643–13658, 2024.
- [Zheng *et al.*, 2023] Wenqing Zheng, SP Sharan, Ajay Kumar Jaiswal, Kevin Wang, Yihan Xi, Dejia Xu, and Zhangyang Wang. Outline, then details: Syntactically guided coarse-to-fine code generation. In *International Conference on Machine Learning*, pages 42403–42419, 2023.

# Supplementary Material

## Design-Specification Tiling for ICL-based CAD Code Generation

### Contents

|          |  |          |
|----------|--|----------|
| <b>A</b> | <b>Theoretical Proofs</b>                    | <b>1</b> |
| <b>B</b> | <b>Test Dataset &amp; ICL Database</b>       | <b>2</b> |
|          | B.1 Complexity Partition . . . . .           | 2        |
|          | B.2 Data Statistics . . . . .                | 2        |
| <b>C</b> | <b>Implementation Details</b>                | <b>2</b> |
|          | C.1 Pseudo Code of DST . . . . .             | 2        |
|          | C.2 Inference-Time Prompt Template . . . . . | 3        |
| <b>D</b> | <b>Baseline ICL Strategies</b>               | <b>3</b> |
| <b>E</b> | <b>Evaluation Details</b>                    | <b>4</b> |
|          | E.1 Evaluation Environments . . . . .        | 4        |
|          | E.2 Evaluation Metrics . . . . .             | 4        |
|          | E.3 Coordinate Alignment . . . . .           | 5        |
| <b>F</b> | <b>Additional Experiments</b>                | <b>6</b> |
|          | F.1 Failure Analysis . . . . .               | 6        |
|          | F.2 More Case Study . . . . .                | 6        |

### A Theoretical Proofs

This section establishes the theoretical foundation of our approach by proving proposition 1, which demonstrates that maximizing the tiling ratio, our proposed surrogate objective for knowledge sufficiency, constitutes a submodular maximization problem.

*Proof.* We first establish notation consistent with the main text. Let  $\mathcal{C}_{\text{query}}$  denote the weighted multi-granular component set of the query  $X_{\text{query}}$ . For an exemplar subset  $S \subseteq \mathbb{N}_n$ , define

$$\mathcal{C}(S) = \bigcup_{i \in S} \mathcal{C}_i \quad (11)$$

as the union of components from all exemplars in  $S$ . The tiling objective (Eq. (7)) is

$$f(S) = w(\mathcal{C}(S) \cap \mathcal{C}_{\text{query}}), \quad (12)$$

where the weighted size function

$$w(\mathcal{C}(\cdot)) = \sum_{n \in \mathcal{N}} n \cdot |\mathcal{C}^{(n)}(\cdot)| \quad (13)$$

assigns weight  $n$  to each  $n$ -gram component. For convenience, define

$$\mathcal{T}(S) = \mathcal{C}(S) \cap \mathcal{C}_{\text{query}}, \quad (14)$$

so that  $f(S) = w(\mathcal{T}(S))$ .

To complete the proof, we establish that  $f(S)$  satisfies non-negativity, monotonicity, and submodularity.

**Non-negativity.** The weighted size function  $w(\cdot)$  sums non-negative terms: each weight  $n \in \mathcal{N}$  is positive and each cardinality  $|\mathcal{C}^{(n)}(\cdot)|$  is non-negative. Therefore,  $w(\mathcal{T}(S)) \geq 0$  for all  $S \subseteq \mathbb{N}_n$ , which implies  $f(S) \geq 0$ .

**Monotonicity.** Consider arbitrary subsets  $A, B \subseteq \mathbb{N}_n$  with  $A \subseteq B$ . By monotonicity of set union,

$$\mathcal{C}(A) = \bigcup_{i \in A} \mathcal{C}_i \subseteq \bigcup_{i \in B} \mathcal{C}_i = \mathcal{C}(B). \quad (15)$$

Intersecting with  $\mathcal{C}_{\text{query}}$  preserves inclusion:

$$\mathcal{T}(A) \subseteq \mathcal{T}(B). \quad (16)$$

Since  $w(\cdot)$  is monotone with respect to set inclusion,

$$f(A) = w(\mathcal{T}(A)) \leq w(\mathcal{T}(B)) = f(B). \quad (17)$$

This establishes monotonicity.

**Submodularity.** We must show that for all  $A \subseteq B \subseteq \mathbb{N}_n$  and  $x \in \mathbb{N}_n \setminus B$ ,

$$f(A \cup \{x\}) - f(A) \geq f(B \cup \{x\}) - f(B). \quad (18)$$

Define the marginal gain

$$\Delta_A(x) := f(A \cup \{x\}) - f(A). \quad (19)$$

Observe that

$$\begin{aligned} \mathcal{T}(A \cup \{x\}) &= \mathcal{C}(A \cup \{x\}) \cap \mathcal{C}_{\text{query}} \\ &= (\mathcal{C}(A) \cup \mathcal{C}_x) \cap \mathcal{C}_{\text{query}} \\ &= \mathcal{T}(A) \cup (\mathcal{C}_x \cap \mathcal{C}_{\text{query}}), \end{aligned} \quad (20)$$

where  $\mathcal{C}_x$  is the component set of exemplar  $x$ . Since  $w(\cdot)$  is additive over disjoint unions, the marginal gain is

$$\Delta_A(x) = w(\mathcal{T}(A \cup \{x\}) \setminus \mathcal{T}(A)). \quad (21)$$

This simplifies to

$$\Delta_A(x) = w((\mathcal{C}_x \cap \mathcal{C}_{\text{query}}) \setminus \mathcal{T}(A)). \quad (22)$$

Similarly,

$$\Delta_B(x) = w((\mathcal{C}_x \cap \mathcal{C}_{\text{query}}) \setminus \mathcal{T}(B)). \quad (23)$$

Since  $A \subseteq B$ , monotonicity yields  $\mathcal{T}(A) \subseteq \mathcal{T}(B)$ . For any fixed set, removing a larger set yields a smaller remainder:

$$(\mathcal{C}_x \cap \mathcal{C}_{\text{query}}) \setminus \mathcal{T}(A) \supseteq (\mathcal{C}_x \cap \mathcal{C}_{\text{query}}) \setminus \mathcal{T}(B). \quad (24)$$

Applying monotonicity of  $w(\cdot)$  gives

$$\Delta_A(x) \geq \Delta_B(x), \quad (25)$$

verifying (18). This establishes submodularity.

All three properties are now proven.  $\square$

## B Test Dataset & ICL Database

We utilize two open-source datasets, Text2CAD [Khan *et al.*, 2024] and GenCAD-Code [Doris *et al.*, 2025], both derived from the foundational DeepCAD [Wu *et al.*, 2021] repository in our study. The original datasets collectively contain approximately 178K samples. Text2CAD respectively inputs multi-view images of the model and its original Json-formatted structural descriptions into a VLM and a LLM. By synthesizing information across these two modalities, the framework annotated professional natural language annotations for each 3D model. And GenCAD-Code automatically convert the original CAD sequence data into executable python scripts.

In our study, the design descriptions and their corresponding rendered CAD digital models are collected from Text2CAD, while the associated executable CAD code are obtained from GenCAD-Code. After filtering entries with missing inputs and removing duplicate samples with identical descriptions, we retained a total of **151940** valid triplets. Each triplet  $\{NL_i, Code_i, CAD_i\}$  consists of a natural language design specification, executable CAD code, and a corresponding rendered CAD digital model.

### B.1 Complexity Partition

We quantify the complexity of each instance using three complementary metrics:

- $\text{Len}(NL_i)$ : the length of the natural language design specification.
- $\text{Geom}(CAD_i)$ : the geometric complexity [Alrashedy *et al.*, 2025], defined as the total number of edges and faces in the CAD model.

- $\text{Ops}(Code_i)$ : the operational complexity of the code, measured by the number of valid operations of Cad-Query code.

To ensure equal contributions from each dimension and to mitigate biases arising from differing scales, all three metrics were standardized using min-max normalization. Then a comprehensive complexity score, denoted as **Complexity<sub>i</sub>**, is construct by aggregating these three normalized metrics as shown in Eq. (26). Finally, samples are ranked by complexity and partitioned into three equal-sized tiers (Easy, Middle, and Hard) as illustrated in Fig. 7. For the final experimental setup, 300 samples were randomly selected from each tier as the test set, while the remaining samples served as the ICL database.

$$\begin{aligned} \mathbf{N}(x_i) &= \frac{x_i - \min(\mathbf{x})}{\max(\mathbf{x}) - \min(\mathbf{x})} \\ \text{Complexity}_i &= \mathbf{N}(\text{Len}(NL_i)) + \mathbf{N}(\text{Geom}(CAD_i)) \\ &\quad + \mathbf{N}(\text{Ops}(Code_i)) \end{aligned} \quad (26)$$

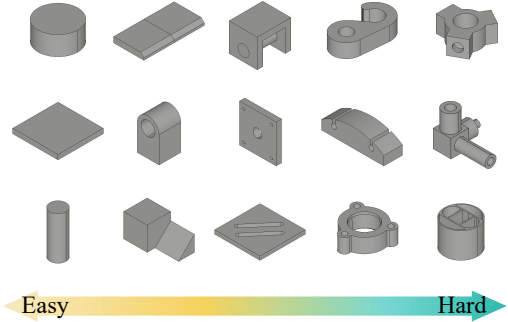


Figure 7: Examples of 3D models ranked by complexity.

### B.2 Data Statistics

To validate the effectiveness of the proposed complexity-based stratification, we computed the aforementioned metrics for each group (**Easy**, **Middle**, and **Hard**). As summarized in Tab. 2, all three dimensions (linguistic, geometric, and operational complexity) exhibit clear increases. These results demonstrate that the integrated scoring system effectively distinguishes varying levels of modeling difficulty, providing a robust foundation for fine-grained performance analysis.

## C Implementation Details

This section provides the pseudo code of of DST and the prompt template used for CAD code generation at inference time.

### C.1 Pseudo Code of DST

Algorithm 1 presents the complete pseudocode for the Design-Specification Tiling (DST) exemplar selection method. The algorithm implements weighted tiling ratio

Table 2: Dataset statistics across complexity groups. For each group, the top row shows the **Mean** and the bottom row shows the **Median**.

| Group  | stat.  | Len( $NL_i$ ) | Geom( $CAD_i$ ) | Ops( $Code_i$ ) | Test Set |
|--------|--------|---------------|-----------------|-----------------|----------|
| Easy   | Mean   | 147.67        | 17.33           | 5.67            | 300      |
|        | Median | 143.00        | 18.00           | 5.00            |          |
| Middle | Mean   | 195.00        | 27.67           | 9.67            | 300      |
|        | Median | 182.00        | 22.00           | 9.00            |          |
| Hard   | Mean   | 327.67        | 51.33           | 21.33           | 300      |
|        | Median | 301.50        | 50.00           | 19.00           |          |

#### Algorithm 1: Pseudocode of DST Algorithm

**Input:** Query design specification components  $C_{\text{query}}$ , exemplar component sets  $\{C_i\}_{i=1}^n$ , selection capacity limit  $k \ll n$ , multi-granular set  $N$ .

**Output:** Subset of exemplar indices  $S^* \subseteq \mathbb{N}_n$  such that  $|S^*| = k$ .

- 1 Initialize the selected set:  $S \leftarrow \emptyset$ ;
- 2 Initialize the covered query components:  $\mathcal{T} \leftarrow \emptyset$ ;
- 3 **for**  $i \leftarrow 1$  **to**  $k$  **do**
- 4      $s \leftarrow -1$ ;  $\text{max\_gain} \leftarrow 0$ ;
- 5     **for**  $j \leftarrow 1$  **to**  $n$  **do**
- 6         **if**  $j \notin S$  **then**
- 7              $\mathcal{T}_{\text{new}} \leftarrow \mathcal{T} \cup (C_j \cap C_{\text{query}})$ ;
- 8              $g \leftarrow w(\mathcal{T}_{\text{new}}) - w(\mathcal{T})$ ; // weighted marginal tiling gain
- 9             **if**  $g > \text{max\_gain}$  **then**
- 10                  $\text{max\_gain} \leftarrow g$ ;
- 11                  $s \leftarrow j$ ;
- 12             **end**
- 13         **end**
- 14     **end**
- 15     **if**  $s = -1$  **then**
- 16         **break**;
- 17     **end**
- 18     // terminate if no positive gain
- 19      $\mathcal{T} \leftarrow \mathcal{T} \cup (C_s \cap C_{\text{query}})$ ; // Update covered components
- 20      $S \leftarrow S \cup \{s\}$ ; // Update selected set
- 21 **end**
- 22 **return**  $S^* = S$ ;

computation and greedy submodular maximization, achieving the  $(1 - 1/e)$ -approximation guarantee established in proposition 1.

## C.2 Inference-Time Prompt Template

At inference time, selected exemplars and their corresponding CAD code are structured into an in-context learning prompt for the language model. The prompt comprises three hierarchical components:

1. **System prompt:** Establishes the model’s role as a CAD code generation expert.
2. **Task instruction:** Specifies output format constraints and generation requirements.

3. **Demonstration sequence:** Presents  $k$  exemplar pairs  $\{(X_i, Y_i)\}_{i=1}^k$  ordered by relevance to the query.

The query specification  $X_{\text{query}}$  is appended as the final input, prompting the model to generate the corresponding CAD code  $\hat{Y}$ . The complete prompt structure follows:

### ICL Prompt Template

#### System Prompt:

You are an expert CAD engineer proficient in Python and the CadQuery library. Your task is to generate precise, executable CadQuery scripts according to given natural language descriptions.

#### Instruction:

Please create a CadQuery Python code which can generate a model based on the instruction and description.

The final CadQuery code MUST BE put in `'''python code'''` with ONLY the executable code inside the python box, nothing else.

Relevant examples will be provided in sequence according to their similarity to the final query, and these examples may be helpful for answer generation.

Please don’t use the non-existent `.scale()` method on Workplane objects.

#Examples Begin:

Description: {Design specification of the first exemplar}

''' {Code of the first example} '''

.....

#Examples End

#### User Input:

Description: {Design specification of the current query}

## D Baseline ICL Strategies

We evaluate several baseline in-context learning (ICL) exemplar selection strategies to benchmark our proposed DST selection strategy. These baselines include similarity-based approaches (e.g., LDSIM and BM25) as well as diversity-oriented techniques (e.g., Diversity). The primary challenge in ICL is selecting an effective context for a given input source code  $X_{\text{query}}$ . This problem can be formalized as selecting a subset of indices  $S$  that satisfies the context size

constraint  $|S| = k$ :

$$S^* = \operatorname{argmax}_{S \subseteq \mathbb{N}_n, |S|=k} \operatorname{Score}(S, X_{\text{query}}). \quad (27)$$

Each exemplar selection method can be viewed as a specific instantiation of the general formulation in Eq. 27.

**(1) Random Sampling (Random):**  $k$  exemplars are uniformly sampled from the candidate pool, independent of the test input  $X_{\text{test}}$ :

$$S^* \sim \operatorname{Uniform}(\mathbb{N}_n), \quad |S^*| = k. \quad (28)$$

**(2) Retrieval by Levenshtein Distance (LDSIM):** Levenshtein distance (LD), also known as edit distance, is a fundamental string metric that quantifies similarity by counting the minimum number of single-character edit operations required to transform one sequence into another. Due to its simplicity and low computational overhead, LD has been widely adopted in prior ICL literature for exemplar retrieval and matching tasks [Shen *et al.*, 2025; Du *et al.*, 2025; Liu *et al.*, 2025b]. The selection score is defined as the negative sum of Levenshtein distances between each exemplar and the test input:

$$S^* = \operatorname{argmax}_{S \subseteq \mathbb{N}_n, |S|=k} - \sum_{i \in S} \operatorname{LD}(X_i, X_{\text{test}}). \quad (29)$$

**(3) Retrieval by Best Matching 25 (BM25):** BM25 is a bag-of-words retrieval function that is widely used in ICL [Chen *et al.*, 2023] to rank textual documents by their relevance to a given query. As a successor to the classic term frequency–inverse document frequency (TF–IDF) algorithm, BM25 addresses key limitations of TF–IDF, such as term frequency saturation, and introduces tunable parameters to adapt to diverse retrieval scenarios. Consequently, BM25 has become a foundational baseline for retrieval tasks. The overall score is computed as the sum of BM25 relevance scores between each candidate and the test input:

$$S^* = \operatorname{arg} \max_{S \subseteq \mathbb{N}_n, |S|=k} \sum_{i \in S} \operatorname{BM25}(X_i, X_{\text{test}}). \quad (30)$$

**(4) Retrieval by Diversity with Clustering (Diversity):** Following prior work [Xiao *et al.*, 2025], we implement a purely diversity-based strategy that partitions the training set into  $k$  clusters using the k-means algorithm and selects the sample closest to each cluster centroid. Cosine similarity computed over CodeBERT embeddings [Feng *et al.*, 2020] is used as the distance metric:

$$\mathbb{N}_n \xrightarrow{\text{k-means}(f_{\text{CB}}(X_i))} \{C_1, \dots, C_k\}, \quad (31)$$

where  $C_j$  denotes the index set of the  $j$ -th cluster.

$$S^*_{[i]} = \operatorname{arg} \max_{j \in C_i} \cos(f_{\text{CB}}(X_j), f_{\text{CB}}(X_{\text{test}})), \quad (32)$$

for  $i \in \{1, \dots, k\}$ , and the final exemplar set is given by  $S^* = S^*_{[1:k]}$ .

## E Evaluation Details

### E.1 Evaluation Environments

**Infrastructure** All experiments in this work are conducted on a high-performance computing workstation equipped with eight NVIDIA A100 Tensor Core GPUs (80 GB HBM2e VRAM per GPU) and an Intel Xeon Platinum 8375C CPU. Our framework is implemented with Python 3.11.5, where the core CAD modeling pipeline is built on CadQuery 2.6.1 and CadQuery-OCF 7.8.1.1.post1 for high-fidelity 3D geometry rendering and geometric validity validation. For the generation from natural language design specifications to executable CadQuery code, we employ state-of-the-art closed-source large language models via their official remote API interfaces.

**CadQuery** In our framework, CadQuery<sup>2</sup> is employed as the core tool for generating 3D CAD models, serving as a lightweight, dependency-free Python-based parametric CAD scripting library. CadQuery constructs 3D geometries through chainable geometric operations (e.g., `box()`, `circle()`, `extrude()`), with all modeling workflows encoded as modular, readable and fully executable Python scripts. By leveraging the CadQuery-OCF kernel, CadQuery scripts provide a complete, modular, and fully executable modeling pipeline that can directly render into high-fidelity 3D models without requiring extra post-processing.

Furthermore, CadQuery is well-suited as an intermediate representation for text-to-CAD generation, with prominent merits including strong editability, high interpretability, and native compatibility with large language models (LLMs). It provides a diverse set of expressive geometric operations spanning basic primitives to complex topological modeling, which accurately match the compositional semantics of natural language design specifications. Leveraging Python as its native syntax, CadQuery aligns seamlessly with LLMs pre-trained on code corpora, facilitating efficient text-driven CAD code generation. Importantly, CadQuery scripts realize gapless unification of human interpretability and machine executability between generated code and the final 3D geometric models.

### E.2 Evaluation Metrics

To evaluate the 3D objects through CAD solid Model, we use three evaluation metrics to compare the quality of the generated 3D object against the ground truth. Following prior works [He *et al.*, 2025; Niu *et al.*, 2025; Guan *et al.*, 2025; Alrashedy *et al.*, 2025; Doris *et al.*, 2025], we use the widely-used four metrics to evaluate model performance.

**Valid Syntax Rate (VSR)** is defined as the percentage of model-generated CadQuery scripts from the test subset that are syntactically valid and return no errors when run as Python files [Doris *et al.*, 2025].

**Intersection over the Union (IoU)** is used to evaluate how closely the generated 3D object P aligns with the ground truth Q [Niu *et al.*, 2025]. As shown in Eq. (33), it calculates the ratio of the intersection area between P and Q to the union

<sup>2</sup><https://cadquery.readthedocs.io/>

area between  $P$  and  $Q$ :

$$IoU(P, Q) = \frac{|P \cap Q|}{|P \cup Q|}. \quad (33)$$

**Chamfer Distance (CD)** is the most commonly used point cloud distance [Alrashedy *et al.*, 2025; He *et al.*, 2025; Guan *et al.*, 2025; Niu *et al.*, 2025]. The IoU measures the overlap of the bounding boxes between the generated and ground truth 3D objects, while point cloud distance metrics are based on the geometric properties (e.g., height, width, and volume) of 3D objects. As shown in Eq. (34), it calculates the average sum of the bidirectional nearest neighbor distances:

$$CD(P, Q) = \frac{1}{2|P|} \sum_{p \in P} \min_{q \in Q} d_{p,q} + \frac{1}{2|Q|} \sum_{p \in P} \min_{q \in Q} d_{p,q}, \quad (34)$$

where  $d_{p,q} = \|p - q\|_2$ ,  $P$  is the generated 3D CAD object and  $Q$  is the ground truth CAD object.

**Edge Chamfer Distance (ECD)** is another point cloud distance, which is a structured variant of Chamfer Distance (CD), specifically designed for wireframes/edge point clouds, to edge line segments by limiting distance calculation, enhancing sensitivity to geometric structures such as corners and edges.

**Handling of Invalid Outputs.** To ensure a rigorous and impartial evaluation across all metrics (IoU, CD, and ECD) we adopt a worst-case penalty for samples where model generation fails or errors occur. Specifically, these invalid outputs are represented as a singleton point set located at the coordinate origin  $(0, 0, 0)$ . Under this convention, the IoU is consistently recorded as 0, while CD and ECD values are calculated based on the distance between the origin point and the ground truth model. Since all target shapes undergo a normalized transformation process prior to evaluation (refer to E.3), these distance-based penalties remain bounded and do not exert a disproportionate influence on the final performance results.

### E.3 Coordinate Alignment

Due to the inherent ambiguity in natural language descriptions regarding reference frames and absolute coordinates, discrepancies in relative position and orientation may exist between the generated solid model and the ground truth shape, denoted as  $P$  and  $Q$ . Furthermore, variations in absolute scale across samples can lead to inconsistent weighting in distance-based metrics. To eliminate these shape-independent biases, we apply a series of rigid transformations (including translation, rotation, and scaling) to normalize and align  $P$  with  $Q$  before metric computation.

**Normalization** sFirst, under the assumption of uniform mass distribution, we translate the centroid of the ground truth model  $Q$  to the coordinate origin. For scaling, we utilize the **radius of gyration** [Lian *et al.*, 2013; Doris *et al.*, 2025] as a dimensional reference. Specifically, we apply uniform scaling such that the mean distance from the model’s differential mass elements to the origin is normalized to a unit

length. The detailed operations are as follows:

$$\begin{aligned} \text{Centroid}(Q) &= \bar{q} = \frac{1}{|Q|} \int_{x \in Q} x \, dx \\ \text{Translate}(Q, -\bar{q}) &= \{x - \bar{q} \mid x \in Q\} \\ R_g(Q) &= \sqrt{\frac{\text{Tr}(I_Q)}{2 \cdot \text{Vol}(Q)}} \\ \text{Scale}(Q, R_g(Q)) &= \left\{ \frac{x}{R_g(Q)} \mid x \in Q \right\} \end{aligned} \quad (35)$$

where  $I_Q$  stands for the inertia matrix of  $Q$  and  $\text{Vol}(Q)$  stands for the volume of  $Q$ .

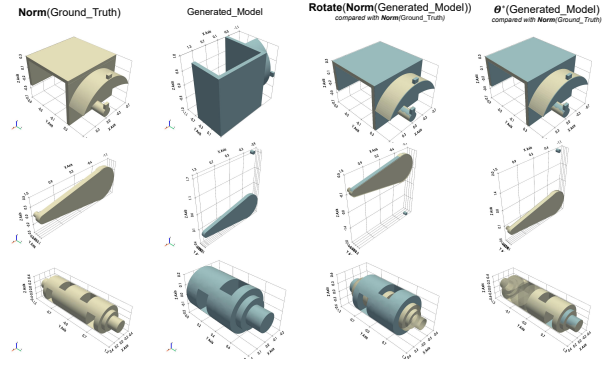


Figure 8: The normalized ground truth  $\text{Norm}(Q)$  and the generated models  $P$  under different transformations: it is observed that when the generated model is substantially consistent with the ground truth, normalization and orthogonal rotation can effectively achieve the optimal alignment. However, in cases where the generated model is only partially correct, a more exhaustive search across a broader range of transformation combinations is necessary.

**Optimal alignment** In practice, simply applying an identical normalization to  $P$  does not guarantee optimal alignment, although it can achieve an optimal result over IoU [Doris *et al.*, 2025]. Therefore, we consider a combinatorial space of operations for  $P$ :

- **Translation & Scaling:** We evaluate two reference sources: the parameters derived from  $P$  itself (self-normalization) or those inherited from  $Q$  (direct alignment). This yields four combinations.
 
$$\begin{aligned} \text{Translate}(P, x), x &\in \{-\bar{q}, -\bar{p}\} \\ \text{Scale}(P, r), r &\in \{R_g(P), R_g(Q)\} \end{aligned}$$
- **Rotation:** We only consider orthogonal alignments with respect to the  $XYZ$  axes (i.e., rotations of  $[0^\circ, 90^\circ, 180^\circ, 270^\circ]$  along the  $x, y,$  and  $z$  axes), resulting in 24 distinct rotation permutations. This exhaustive search over the discrete set of orientations ensures that the models are compared in their optimal orthogonal alignment.

By evaluating these  $4 \times 24 = 96$  candidate combinations, the optimal transformation  $\Theta^*$  is determined by:

$$\Theta^* = \arg \max_{\Theta \in \Omega} \text{Metric}(\Theta(P), \text{Norm}(Q)) \quad (36)$$

where  $\Omega$  denotes the set of 96 transformation candidates, the transformation that yields the highest similarity score, which considers both volumetric alignment (IoU) and surface fidelity (CD), is retained as the optimal alignment for evaluation. Example of different transformation is shown in Fig. 8.

## F Additional Experiments



Figure 9: Failures distribution of DeepSeek-V3: The table (bottom) shows the count of each error types, while the pie charts (top) visualize the percentage of Error Type under Zeroshot, Random, LDSIM, and DST settings.

### F.1 Failure Analysis

Throughout the pipeline {source code extraction, compilation and execution, 3D rendering}, the encountered failures can be systematically classified into the following three categories:

- **Type I: Response and Syntax Errors.** These failures primarily occur during the initial code extraction phase. Such errors typically stem from inconsistent input/output formats or malformed code blocks that fail to adhere to the required syntax.
- **Type II: API Misuse and Semantic Errors.** This category involves the invocation of non-existent attributes or the passing of invalid arguments to CadQuery methods. These issues reflect the model’s deficiency in domain-specific knowledge regarding the precise implementation details of third-party libraries.
- **Type III: Geometric Constraint Violations.** These are logical failures where the generated code violates fundamental geometric rules, leading to runtime crashes. Representative cases include: No pending wires present (i.e.,

Table 3: Failures distribution of DeepSeek-V3: The table shows the count of each error types under Zeroshot, Random, LDSIM, and DST settings(5-shot).

| Failure Type             | Zeroshot   | Random    | LDSIM     | DST       |
|--------------------------|------------|-----------|-----------|-----------|
| TYPE I:Syntax Error      | 10         | 3         | 0         | 1         |
| TYPE II:API Misuse       | 114        | 12        | 4         | 5         |
| TYPE III:Geometric Error | 51         | 43        | 22        | 23        |
| Others                   | 10         | 5         | 2         | 4         |
| <b>Total Counts</b>      | <b>185</b> | <b>63</b> | <b>28</b> | <b>33</b> |

attempting to create a solid from a non-contiguous path), Null-Entity Operations (i.e., extruding an empty point set), Non-coplanar operations (i.e., performing union or subtraction on workplanes that do not share the same plane).

Taking DeepSeek-V3 as a representative case, the distribution of these error types across different input configurations is illustrated in Fig. 9.

Through a comparative analysis of the error distributions across the four experimental groups, two key insights emerge regarding the relationship between in-context learning and failure distribution: first the significant reduction in **Type II** (API Misuse) errors in the three few-shots groups (compared to the Zeroshot baseline) suggests that providing sufficient exemplars can largely rectify the model’s misuse of third-party libraries. Despite the overall improvement in success rates provided by LDSIM and DST, these methods remain insufficient for resolving **Type III** (Geometric Error). This suggests that Type III errors typically arise from intricate combinatorial logic and spatial reasoning that cannot be easily acquired through partially similar examples.

### F.2 More Case Study

As illustrated in Fig. 10, more case study was conducted among different strategies using three representative LLMs: Qwen3-A3B, DeepSeek-V3, and Claude4.5-Haiku.

The top row presents the ground truth, with the rows below corresponding to the 3D CAD object generation outputs of the respective models under various strategies. As demonstrated in Fig. 10, among all in-context learning (ICL) strategies evaluated, the Dialogue State Tracking (DST) approach consistently outperforms other methods across the three representative LLMs.

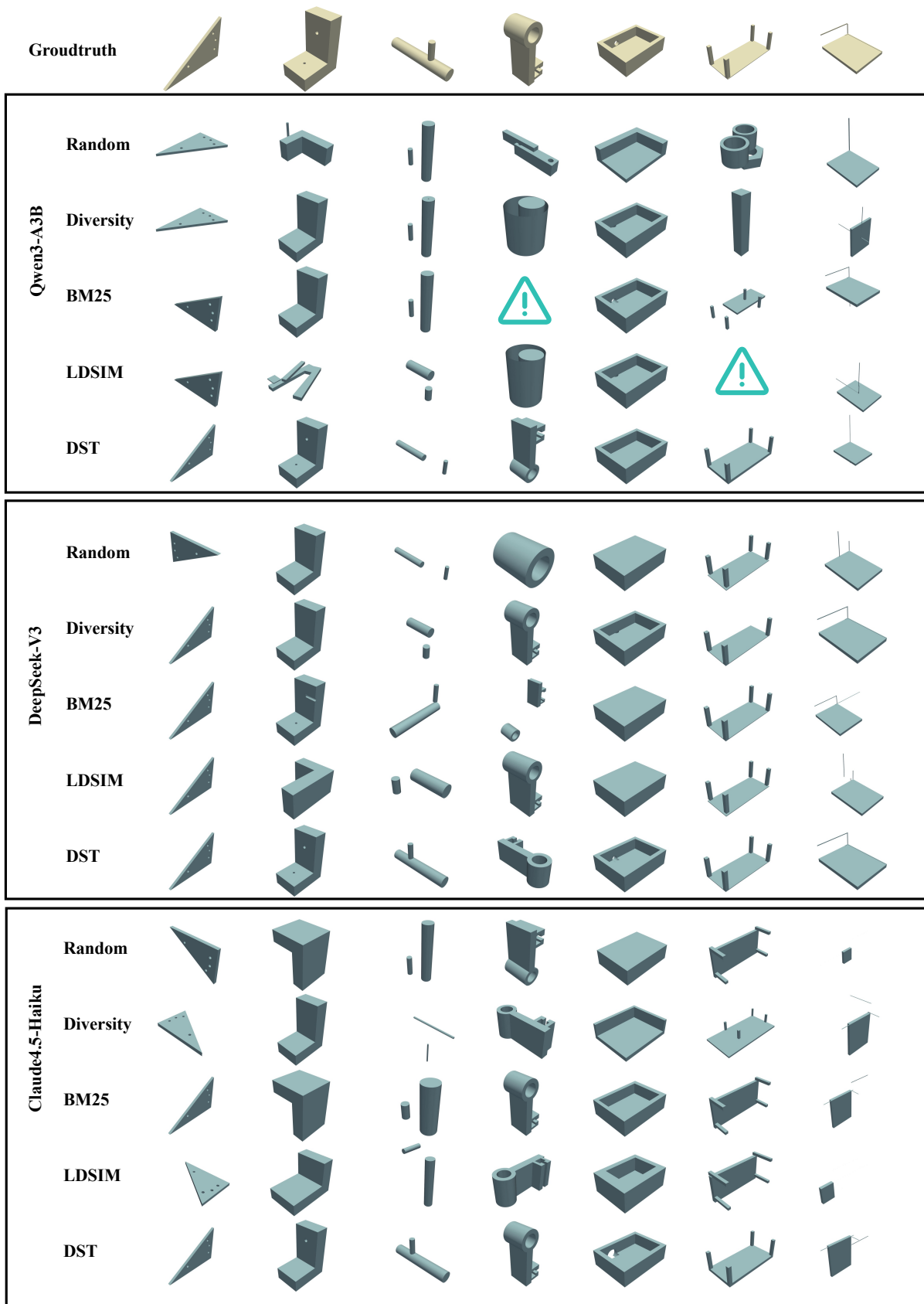


Figure 10: 3D CAD objects generated by All three Models using different methods, where exclamation marks indicate the CAD code unable to produce valid CAD objects.